In Vivo Targeted Deep-Tissue Photodynamic Therapy Based on Near-Infrared Light Triggered Upconversion Nanoconstruct

Sisi Cui,[†] Deyan Yin,[†] Yuqi Chen,[†] Yingfeng Di,[†] Haiyan Chen,[†] Yuxiang Ma,[†] Samuel Achilefu,[‡] and Yueqing Gu[†,*]

[†]Department of Biomedical Engineering, School of Life Science and Technology, State Key Laboratory of Natural Medicines, China Pharmaceutical University, Nanjing, 210009, P. R. China and [‡]Department of Radiology, School of Medicine, Washington University, St. Louis, Missouri, United States

ABSTRACT

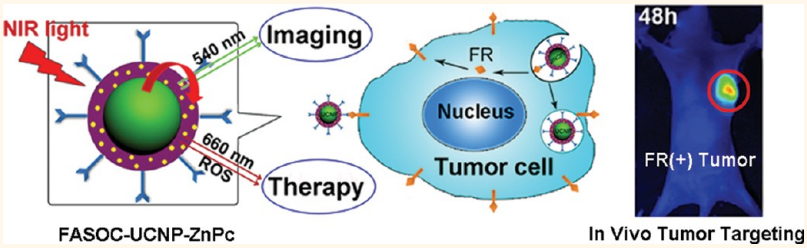

Two major challenges of current photodynamic therapy (PDT) are the limited tissue penetration of excitation light and poor tumor-selectivity of the photosensitizer (PS). To address these issues, we developed a multifunctional nanoconstruct consisting of upconversion nanoparticles (UCNPs) that transform near-infrared (NIR) light to visible light and a photosensitizer zinc(II) phthalocyanine (ZnPc). Folate-modified amphiphilic chitosan (FASOC) was coated on the surface of UCNPs to anchor the ZnPc close to the UCNPs, thereby facilitating resonance energy transfer from UCNPs to ZnPc. Confocal microscopy and NIR small animal imaging demonstrated the enhanced tumor-selectivity of the nanoconstructs to cancer cells that overexpressed folate receptor. Reactive oxygen species (ROS) generation in cancer cells under a 1-cm tissue was higher upon excitation of UCNPs with the 980 nm light than that with 660 nm irradiation. *In vivo* PDT treatments for deep-seated tumors demonstrated that NIR light-triggered PDT based on the nanoconstructs possessed remarkable therapeutic efficacy with tumor inhibition ratio up to 50% compared with conventional visible light-activated PDT with a noticeable reduced tumor inhibition ratio of 18%. These results indicate that the multifunctional nanoconstruct is a promising PDT agent for deep-seated tumor treatment and demonstrate a new paradigm for enhancing PDT efficacy.

KEYWORDS: upconversion · tumor-targeting · folate receptor · deep-tissue · photodynamic therapy

Photodynamic therapy (PDT) is a therapeutic modality that employs a photosensitizer (PS), an appropriate excitation light, and oxygen molecules for local treatment of diseases. Although PDT has emerged as a viable treatment option for early stage cancer and an adjuvant for surgery in late-stage cancer, some obstacles in clinical adoption of PDT still persist.[1−4] One of the major challenges is the inaccessibility of visible light to the deep-seated tumors. This drawback is caused by irradiating currently approved photosensitizers (PSs) below 700 nm, where light penetration is only a few millimeters from tissue surface. Another limitation is the difficulty in formulating PS in physiological mediums because of their high lipophilicity. In addition, the poor selectivity of conventional PSs for the targeted pathologic sites minimizes PDT efficacy *in vivo* and increases the potential phototoxicity to normal tissues. To improve current PDT, it is important to optimize the solubility of PS molecules in aqueous mediums and shift their excitation wavelength to the near-infrared (NIR) range for deep tissue treatment.

Recent development of upconversion nanoparticles (UCNPs) capable of converting

* Address correspondence to guyueqing@hotmail.com.

Received for review October 20, 2012 and accepted December 18, 2012.

Published online December 18, 2012
10.1021/nn304872n

NIR light into UV−visible light has remarkably facilitated the delivery of light to deep tissue and allowed the use of PDT to treat lesions that were not accessible to visible light. UCNP-based PDT agents require the attachment of an appropriate PS with an excitation band matching the emission of the UCNP.[5−7] Upon excitation of the UCNPs with the NIR light, the ensuing fluorescence resonance energy transfer (FRET) to the attached PS produces cytotoxic reactive oxygen species (ROS) that kills the surrounding cells.[8,9] Unlike the current PDT method, the NIR-to-visible UCNP-based PDT nanoconstruct has several advantages, including (i) the use of NIR irradiation (700−1000 nm) for deep tissue treatment, (ii) reduced autofluorescence, which improves signal-to-noise ratio and noninvasive detection sensitivity, and (iii) the higher hydrophilicity and selectivity of PSs by their encapsulation into UCNP-based targeted carriers without the need for structural modification of PS molecules.

Recently, many nanostructured systems have been used to deliver hydrophobic PSs to tumors.[10−14] These delivery systems enable selective accumulation of PSs within tumors in therapeutic concentrations by passive or active targeting, with little or no uptake by nontumor cells. Among them, polymer or silica modified UCNP-based PDT nanocomplexes have served as both PS carriers and light transducer to PS.[15−18] In this study, a chitosan derivative was used to modify the surface of the hydrophobic UCNPs and efficiently trap the PSs for FRET-mediated PDT. In addition to good biocompatibility, chitosan is also biodegradable and provides a hydrophilic environment for solubilizing the nanoconstructs.

Three common strategies used to incorporate PS to UCNP are physical encapsulation, physical adsorption, and covalent conjugation.[16−19] The physical adsorption method suffers from low loading capacity and premature release of PS from UCNP during the circulation in the blood. Although covalent conjugation of PS to UCNP can effectively eliminate the leakage of PS from UCNPs and ensure energy transfer efficiency between PS and UCNP, it has not yet been used for *in vivo* PDT because of the limited drug loading capacity. In a recent report, physical adsorption of Ce6 onto the UCNP and chemical conjugation of Ce6 to UCNP were combined to maximize the loading of Ce6 on the UCNPs and the PDT efficiency.[18] On one hand, this combined method can increase the loading capacity of PSs to UNCPs compared with the covalent conjugation itself. On the other hand, chemical conjugation may reduce the leakage of Ce6 from the nanoparticle and shorten the distance between Ce6 and UCNPs which can maximize the FRET efficiency. Physical encapsulation to load PSs onto the UCNPs through hydrophobic interaction has been demonstrated to possess the highest drug loading capacity (8−10 wt %) until now.[15,17] However, the higher loading capacity of PSs does not guarantee a better PDT efficiency because an optimized concentration of PSs exists. Here, we loaded hydrophobic ZnPc into the hydrophobic layer of FASOC-UCNPs by physical encapsulation and controlled the loading amount of ZnPc to get a reasonable PDT efficiency.

Diverse UCNP-based PDT agents have been developed for *in vivo* cancer treatment. However, only a few of them were utilized for *in vivo* PDT treatment through intratumoral injection. This inefficient route of administration was needed to obtain higher PDT efficiency and fewer side effects because of the limited tumor specificity and selectivity of previously reported UCNPs.[17,20] Unfortunately, local injection of PDT agents does not disperse the nanoparticles uniformly in the tumor and this technique is less efficient for tumors in deep tissue. Since the passive targeting of UCNP-based PDT nanoparticles is not adequate for *in vivo* PDT treatment through systemic administration, the modification of active targeting ligands to the nanocomplexes is urgently needed to increase local concentration of PSs in tumors and avoid side effects. This can be achieved by the use of folic acid (FA), which has a high affinity to folate receptor (FR) overexpressed in diverse cancer cells. The demand for FA markedly increases during cellular activation and proliferation in malignant tumors. Previous studies have shown that glycosyl-phosphatidylinositol-anchored FR mediates the selective uptake of folate derivatives into the target cells by endocytosis. Importantly, the recycling of FRs in the target cells allows the regenerated receptor to capture and internalize additional FA derivatives into cells.[21] In this work, we applied the FA-modified chitosan (FASOC) to coat UCNPs and encapsulate PSs to constitute a PDT system for deep-tissue treatment. The tumor-targeted FASOC-modified upconversion nanoconstruct (FASOC-UCNP) loaded with ZnPc is designed to selectively accumulate in tumors and to activate the adjacent ZnPc, producing photodynamic therapeutic effects after NIR irradiation.

RESULTS

Synthesis and Characterization of UCNP-Based PDT System. The oleic acid-capped NaYF4:Yb,Er (OA-UCNPs) was synthesized by a solvothermal method in high boiling 1-octadecane solvent.[22] Separately, the FA carboxyl group was conjugated to the amino groups of the amphiphilic *N*-succinyl-*N*′-octyl chitosan (SOC). The resulting FASOC was subsequently coated on the surface of UCNPs *via* hydrophobic interaction between the octadecyl groups of OA-UCNPs and octyl groups of FASOC (Figure 1A) to produce a water-soluble nanoconstruct. Finally, ZnPc photosensitizer was loaded into the FASOC layer of the UCNP core through hydrophobic interaction. Upon 980 nm NIR light irradiation, the red emission (660 nm) from UCNP activated the

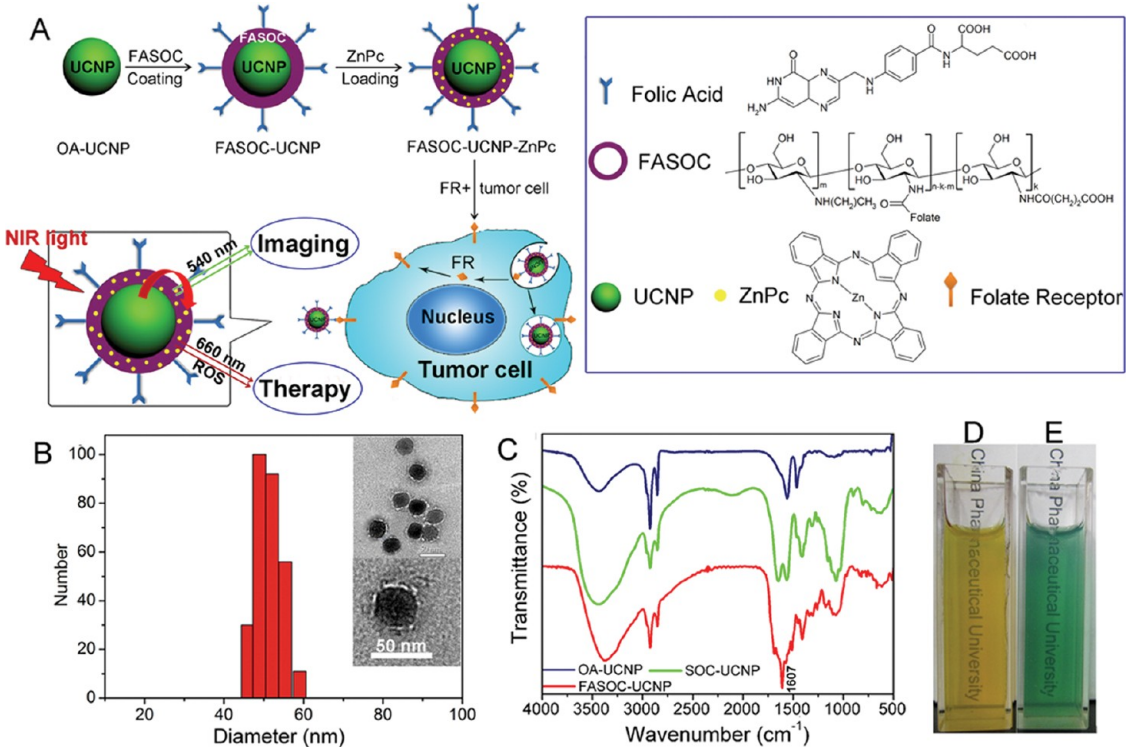

Figure 1. Synthesis and characterization of FASOC-UCNP nanoconstruct. (A) Schematic of the synthesis of FASOC-UCNP-ZnPc nanoconstruct and folate-mediated binding of tumor cells with folate receptor expression; (B) particle size of the prepared nanoconstruct by DLS and TEM measurement; (C) Fourier transform infrared (FTIR) spectra of OA-UCNP, SOC, and FASOC-UCNP; (D) photos of FASOC-UCNP, and (E) ZnPc-loaded FASOC-UCNP in PBS under ambient light.

trapped ZnPc to generate cytotoxic ROS through FRET from UCNP (donor) to ZnPc (acceptor). Meanwhile, the green upconversion luminescence (UCL) from the nanoconstruct can be used for cell imaging. The size of the UCNP-based core/shell nanoconstruct was measured by dynamic light scatter (DLS) and transmission electron microscope (TEM) (Figure 1B). The inner OA-UCNP core (dark color) was ~35 nm and the overall size of the ZnPc-loaded FASOC-UCNPs was approximately 50 nm in diameter after being coated with FASOC as observed in the TEM images (inset). Particle size distribution of FASOC-UCNP on the basis of number-average was ~52.8 nm as determined by DLS measurement. Fourier transform infrared (FTIR) spectra (Figure 1C) showed a new peak at 1607 cm^{-1} for FASOC-UCNP, which was assigned to the −C═N stretching vibration of the pterin ring of FA molecules. This demonstrated the existence of FA in the nanoconstruct. A stable transparent solution was obtained by dispersion of the FASOC-coated UCNPs in aqueous medium (Figure 1D). Formation of a green transparent solution of the ZnPc-loaded nanoconstructs confirmed the entrapment of ZnPc molecules in the FASOC-UCNPs (Figure 1E).

The distinct absorption spectra of different components in the nanoconstruct further supported the conjugation of FA on the nanoconstruct (Figure 2A). After modifying FA ligands, new absorption peaks appeared at 280 and 360 nm, which coincide with the absorption bands of free FA. A similar spectral analysis of FASOC-UCNP-ZnPc showed an obvious absorption band from 600 to 750 nm (Figure 2B), assigned to the absorption of ZnPc, which overlapped with the red emission from $NaYF_4$:Yb,Er UCNPs peaked at 660 nm. The maximum absorption peak of free ZnPc in ethanol centered at 670 nm, but the maximum absorption of FASOC-UCNP-ZnPc varied in aqueous solution at different concentrations of ZnPc loaded in the nanoconstructs. The maximum absorption of FASOC-UCNPs loaded with 150 μg/mL ZnPc was ~670 nm. By contrast, the maximum absorption of FASOC-UCNPs loaded with 250 μg/mL ZnPc was ~610 nm, suggesting that excess amount of ZnPc in the nanoconstructs form aggregates in aqueous solution. For subsequent *in vivo* imaging, a NIR fluorescent dye ICG-Der-01 (Cypate; Figure 2E) synthesized in our lab and the chemical structure of ICG-Der-01was encapsulated in the FASOC-UCNPs.[23] Spectral analysis showed that the resulting FASOC-UCNP-ICG possessed an absorption band from 700 to 830 nm. As shown in Figure 2C, FASOC-UCNPs emitted green (540 nm) and red (660 nm) UCL fluorescence under 980 nm excitation. The surface modification by FASOC slightly decreased the UCL emissions of UCNPs. Since ZnPc absorption overlaps with the red UCL emission from UCNP, the red emission of FASOC-UCNPs was significantly quenched after loading 400 μM ZnPc, suggesting FRET from UCNP to ZnPc (Figure 2C). Thus, the UCL of UCNPs was capable

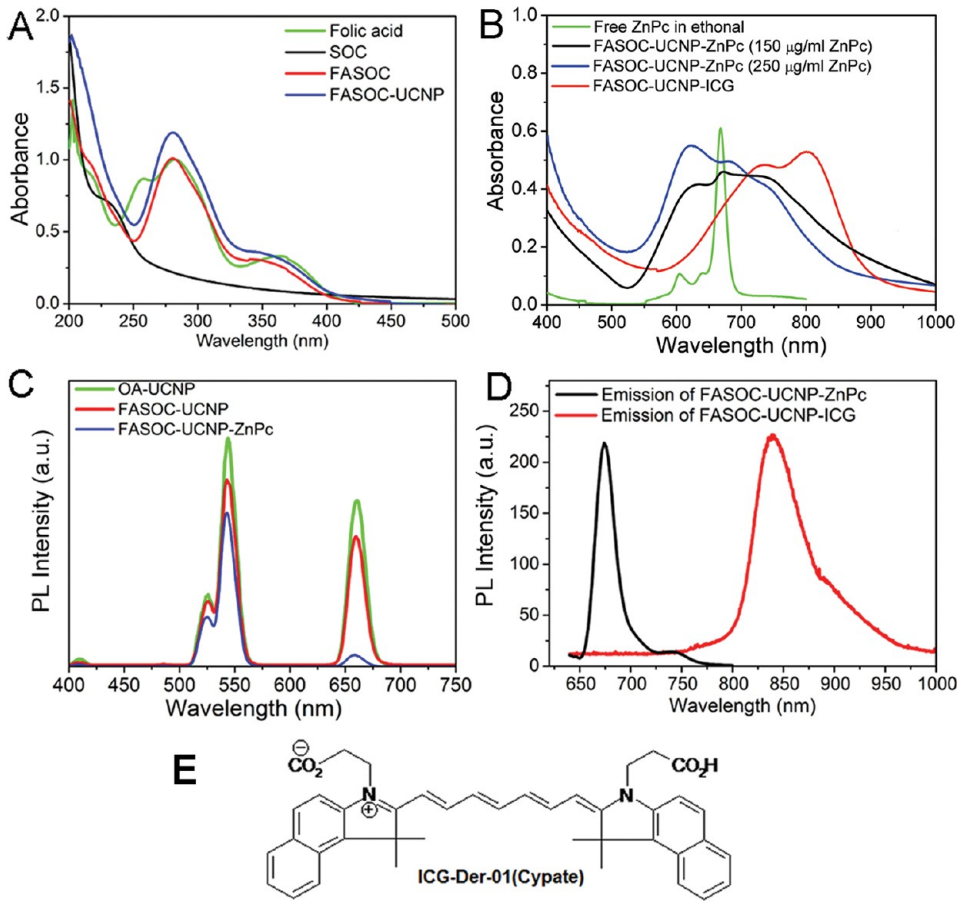

Figure 2. Optical properties of ZnPc and ICG dye-loaded FASOC-UCNP nanoconstructs. (A) Absorption spectra of folic acid (FA), SOC, FASOC, and FASOC-UCNP; (B) Absorption spectra of free ZnPc in ethanol and FASOC-UCNPs loaded with ZnPc (150 or 250 μg/mL) and ICG-Der-01 in aqueous solution; (C) UCL emission spectra of OA-UCNP, FASOC-UCNP, and FASOC-UCNP-ZnPc; (D) fluorescence emission of FASOC-UCNP-ZnPc (λ_{ex} = 610 nm) and FASOC-UCNP-ICG (λ_{ex} = 765 nm); (E) chemical structure of NIR fluorescence dye ICG-Der-01.

of activating the ZnPc to produce cytotoxic ROS (such as singlet oxygen, superoxide anions and hydroxyl radicals) for tumor treatment. Interestingly, the loaded ZnPc molecules could emit red fluorescence at 670 nm upon 610 nm irradiation, which can be fully utilized in confocal fluorescence imaging. Additionally, the NIR emission from ICG centered at 840 nm was detected when FASOC-UCNP-ICG was exposed to 765 nm NIR light, which is optimal for *in vivo* imaging (Figure 2D).

ZnPc loading capacity and encapsulation efficiency were quantitatively measured by fluorescence spectrophotometry.[20,24] As shown in Figure 3A, the ZnPc loading capacity increased with ZnPc concentration and attained saturation at 10% of ZnPc/nanoconstruct, when ZnPc concentration reached 346 μg/mL (600 μM). The loading plateau represents the amount of ZnPc in the nanoconstructs that was close to saturation, and excess ZnPc may hardly be entrapped into the nanoconstructs. Encapsulation efficiency of ZnPc in the FASOC-UCNPs gradually reduced with a further increase in ZnPc concentration (Figure 3B). When the added ZnPc concentration in FASOC-UCNP-ZnPc was less than 57 μg/mL (100 μM), the encapsulation efficiency was above 90%, but the ZnPc loading capacity was below 3%. There was a marked decrease in the encapsulation efficiency (to less than 80%) when the ZnPc was present at more than 288 μg/mL (500 μM). The minimal encapsulation efficiency was about 65% at the ZnPc saturation condition. Encapsulation efficiency and loading capacity of the nanoparticles were affected by the initial ZnPc concentration. The increase in the initial ZnPc concentration led to a decrease of encapsulation efficiency and an enhancement of loading capacity (Figure 3 panels A,B).

The release profiles of ZnPc from FASOC-UCNPs at various pH values (Figure 3C) indicated the release rate of ZnPc within 50 h was highest when the nanoconstructs were dispersed in pH 5.7 phosphate buffer (containing 2% SDS), and was lowest in pH 7.4 phosphate buffer (containing 2% SDS). The results indicate that the loading of ZnPc through the intermolecular hydrophobic force is sensitive to the pH, because amphiphilic chitosan can dissolve in acidic solutions of pH below 6.5. Less than 20% of ZnPc was detached from FASOC-UCNPs even at pH 5.7 after 50 h incubation at 37 °C, which implied that the leakage of ZnPc

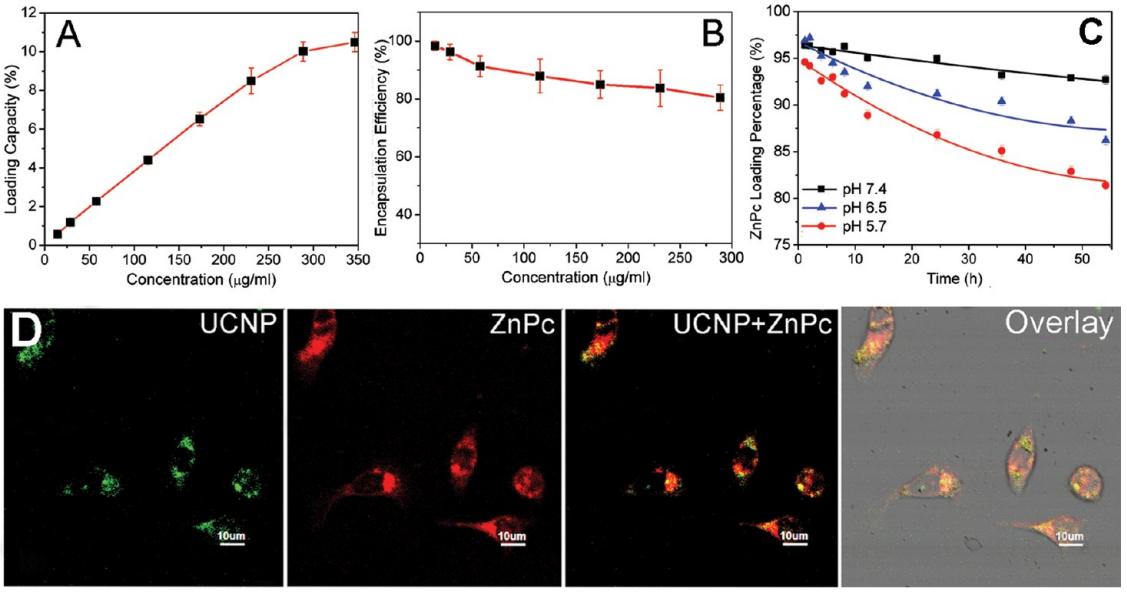

Figure 3. ZnPc loading and encapsulation efficiency in FASOC-UCNPs and the stability of ZnPc in the nanoconstructs in PBS solution and cancer cells: (A) determination of ZnPc loadings at different ZnPc concentrations; (B) encapsulation efficiency of ZnPc in FASOC-UCNPs at different ZnPc concentration; (C) the ZnPc release from the FASOC-UCNP-ZnPc in phosphate buffer at different pH values (5.7, 7.4 and 8.0) containing 2% SDS; (D) intracellular uptake of FASOC-UCNP-ZnPc in cancer cells, indicating the colocolization of ZnPc and UCNPs inside cells.

from the nanoconstructs can be effectively minimized by an FASOC coating in a physiological environment. Co-localization of the UCNPs (green fluorescence) and ZnPc (red fluorescence) in Bel-7402 cells using confocal fluorescence imaging indicated an intrinsic association of the UCNPs with the ZnPc inside cells (Figure 3D). The good stability of the prepared nanoconstruct in physiological solution and cells ensures the effective FRET for PDT treatment.

***In Vitro* Cytotoxicity, Tumor-Targeting to Cancer Cells and ROS Production.** Cytotoxicity of the UCNP-based nanoconstruct is an important consideration for materials intended for *in vivo* application. Toward this goal, assessment of cell viability of HELF cells and MDA-MB-231 cancer cells were examined. Incubation with FASOC-UCNP-ZnPc showed that there was minimal decrease in cell viability (<5%), even when HELF and MDA-MB-231 cells were incubated with 200 μg/mL of FASOC-UCNP-ZnPc for 48 h (Supporting Information, Figure S1). This cytotoxicity study demonstrates that FASOC-UCNP itself possesses low toxicity without light irradiation.

FR expression levels of each cell line were determined by using RT-PCR, as shown in Supporting Information, Figure S2. The RT-PCR results showed that the FR expression levels on the different cancer cells decrease in the following order: Bel-7402 > MDA-MB-231 > A549. FR expression in the murine S180 cell line was additionally studied by using a different primer in the PCR process. The data exhibited high FR expression on the murine S180 cell line. We were unable to compare the FR expression level in these cells with that of human tumor cells because of the use of different PCR primers. To assess the targeting ability of the nanoconstruct, the ZnPc-loaded FASOC-UCNPs were incubated with different cancer cells (Bel-7402, MDA-MB-231 and A549) expressing different levels of FR and the fluorescence of ZnPc was monitored at different incubation time points (Figure 4A). Red fluorescence of ZnPc and blue emission of Hoechst for cell nucleus staining were simultaneously observed in Bel-7402 and MDA-MB-231 cells with elevated FR expression (FR-positive) after 1 h incubation. The fluorescence signals inside cells gradually enhanced with an increase of the incubation time. ZnPc fluorescence was mainly observed in the cytoplasm region after 10 h incubation. However, the ZnPc fluorescence signals in FR-negative A549 cells were much lower than that in FR-positive cells at the same time point. Semiquantitative fluorescence intensity analysis of ZnPc in these cells confirmed the higher uptake of FASOC-UCNP-ZnPc in FA-positive cells than in the negative cells (Figure 4B). Receptor blocking experiments were carried out to study the uptake mechanism of FA modified nanoconstruct *via* FR mediation. Free FA was first added into the FR-positive Bel-7402 and MDA-MB-231 cells before incubation with the nanoconstruct. Figure 4C shows that fluorescence signals of ZnPc dramatically reduced in FR-positive cancer cells when FRs were initially blocked by excess FA, which can inhibit cellular uptake of FASOC-UCNP-ZnPc. Semiquantitative fluorescence analysis in Bel-7402 or MDA-MB-231 cells demonstrated that there were significant differences ($p < 0.05$) in the cellular uptake of ZnPc between nonblocked cells and FR-blocked cells (Figure 4D).

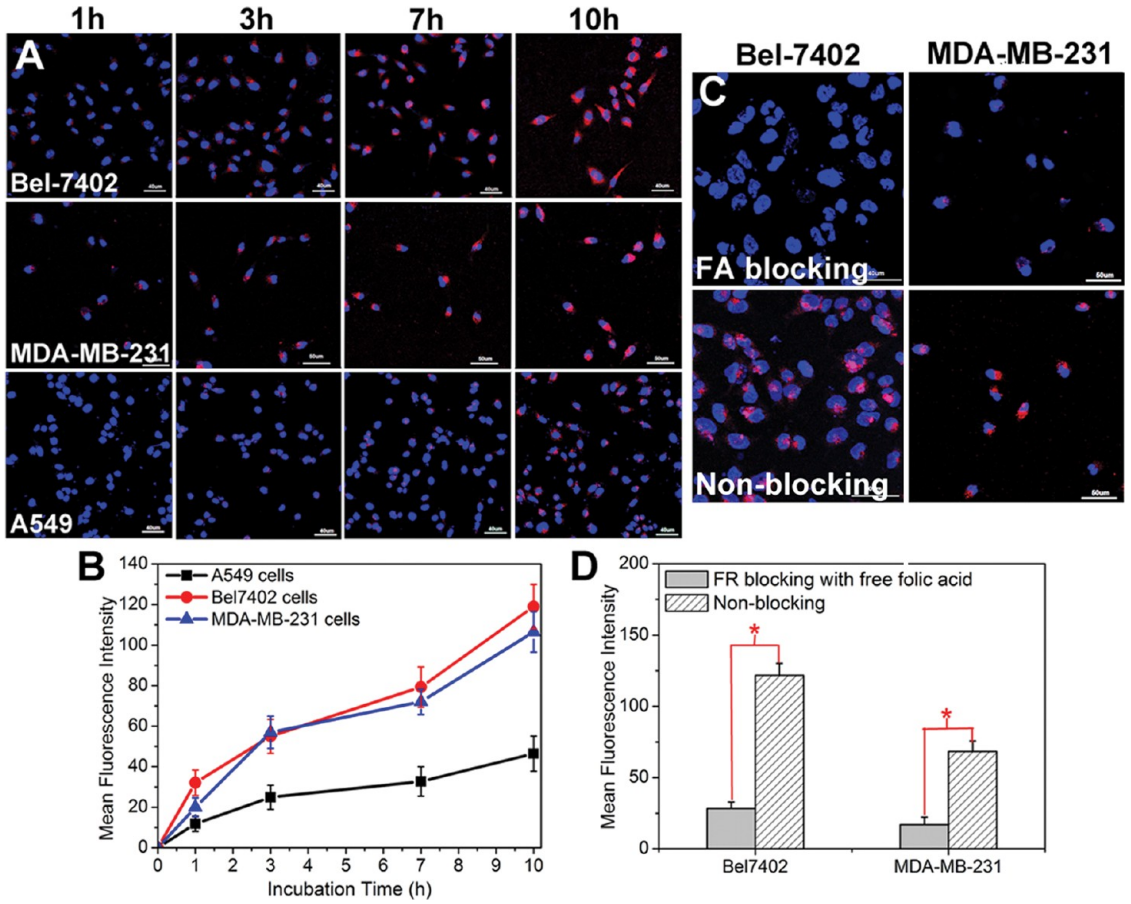

Figure 4. Tumor-targeted ZnPc delivery by the prepared nanoconstructs in cancer cells: (A) dynamics of ZnPc delivered by FASOC-UCNPs in Bel-7402 and MDA-MB-231 cells with FR overexpression and FR-negative A549 cells at different incubation time points; (B) fluorescence intensity of ZnPc determined in Bel-7402, MDA-MB-231, and A549 cells; (C) FR blocking experiments in Bel-7402 and MDA-MB-231 cells; (D) mean fluorescence intensity of ZnPc determined in Bel-7402 and MDA-MB-231 with FR-blocking or nonblocking.

To evaluate the therapeutic efficacy of the UCNP-based PDT system, ROS productions by UCNPs nanoconstruct in physiological solution and inside cancer cells were detected by using DPBF and DCFH-DA probes, respectively.[13] Supporting Information, Figure S3A represents ROS production by FASOC-UCNPs with different loading concentrations of ZnPc determined by DPBF. The optimal concentration of ZnPc in the FASOC-UCNP nanoconstructs was determined to be 150 μg/mL. As shown in Supporting Information, Figure S3B, in control experiments without light irradiation, no obvious change of DPBF absorption was detected. When a solution of the nanoconstruct was directly exposed to the excitation light at different wavelengths, the FASOC-UCNP-ZnPc irradiated by 660 nm light produced more ROS (~68%) than 980 nm light (~53%) for 5 min at the same optical power. To investigate the penetration advantage of the NIR light, thick pork tissue (adipose tissue) was used to mimic living tissue for deep-tissue PDT treatment. Once the FASOC-UCNP-ZnPc solution was covered by 1-cm pork tissues, ROS generation of UCNP-based PDT under 660 nm excitation significantly reduced by ~53%, while it only decreased by ~17% upon 980 nm light irradiation through the 1-cm thick tissues. Similar results of ROS productions were observed in Bel-7402 cells incubated with FASOC-UCNP-ZnPc by using DCFH-DA fluorescent probe (Figure 5). As shown in Figure 5B,D, strong green fluorescence of DCFH was observed in cancer cells under direct 660 or 980 nm irradiation, whereas control cells showed negligible DCFH fluorescence and bright red emission of ZnPc (Figure 5A). After blocking the excitation light with 1-cm pork tissue, fluorescence signals of DCFH in 660 nm light-treated cells (Figure 5C) decreased significantly compared with that in 980 nm light treated cells (Figure 5E). This implies that less ROS was produced by 660 nm light in tissue. Additionally, the red fluorescence of ZnPc dramatically reduced in all PDT treatment groups compared with control cells, which might be caused by photobleaching or photoinactivation under light irradiation.[25]

***In Vivo* Acute Toxicity, Tumor-Targeting, and Deep-Tissue Therapeutic Efficacy.** In the acute toxicity study, 100%, 40%, and 20% deaths were recorded for the mice that received 220, 150, and 105 mg/kg, respectively, on the 7th day after intravenous injection of the nanoconstruct (Supporting Information, Table S1). The median

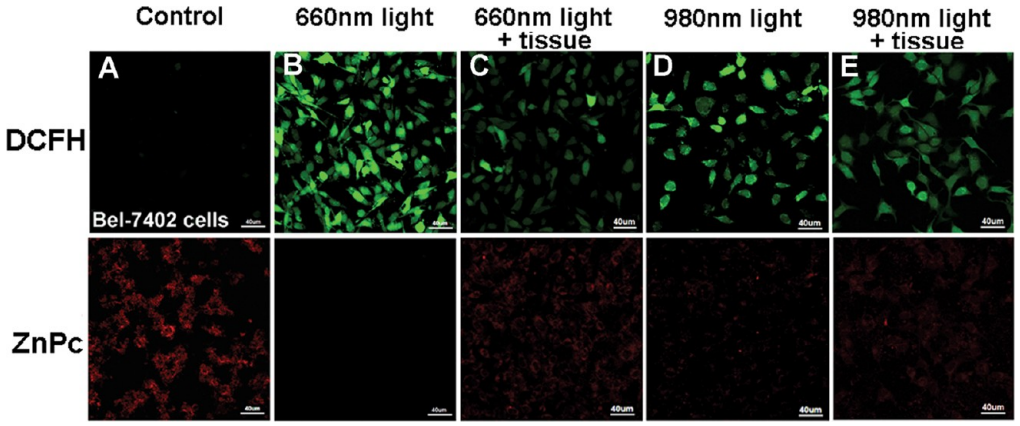

Figure 5. Detection of intracellular reactive oxygen production (ROS) by DCFH-DA staining in Bel-7402 cells incubated with FASOC-UCNP-ZnPc. (A) Control cells without light excitation; (B) ROS production in cells exposed to 660 nm light directly and (C) through a 1-cm tissue; (D) ROS production in cells induced by direct 980 nm irradiation and (E) excited by 980 nm light though a 1-cm tissue.

lethal dosage (LD50) of FASOC-UCNP was determined to be approximate 149 mg/kg (containing 77.5 mg/kg UCNPs). Body weight of mice in both the control and treated groups slightly increased with time (Supporting Information, Figure S4A). Biochemical parameters, including alanine aminotransferase (ALT), aspartate aminotransferase (AST), blood urea nitrogen (BUN), and creatinine (CREA) were investigated to determine the potential side effects of FASOC-UCNP (Supporting Information, Figure S4B). Because all of the mice injected with 220 mg/kg nanoconstruncts were dead within 7 days, biochemical parameters in this group were not detected at day 7, implying the potentially higher toxicity of the nanoconstructs at this dose. The result shows that at day 7, the ALT and AST levels of mice that received 150 mg/kg of FASOC-UCNPs are higher than those of the control group, suggesting the potential hepatic injury at high doses of the nanoconstruct treatment. No significant difference in the BUN and CREA levels in the blood of the control and treated mice were observed, which indicated that no obvious kidney and heart toxicity was induced by FASOC-UCNP. Tissue slices of major organs (liver, kidney and lung) with H&E staining (Supporting Information, Figure S4C) suggest that animals treated with 51 and 105 mg/kg of FASOC-UCNP did not cause any noticeable toxic effect within 7 days post-treatment, but mild edema and a few chronic inflammatory cells were observed in the mice treated with 150 mg/kg FASOC-UCNPs. These results indicated that the acute toxicity of the prepared nanoconstructs was dose-dependent.

To track the biodistribution and tumor targeting ability of the nanoconstruct, ICG was encapsulated into the nanoconstruct for *in vivo* NIR imaging. Supporting Information, Figure S5A shows that the FASOC-UCNP-ICG first accumulated in the liver before gradual excretion into the intestines within 24 h postinjection in nontumor bearing mice. After 48 h, nanoconstruct was virtually cleared from the body through enterohepatic circulation, as evidenced by enhanced NIR fluorescence in the feces. To ascertain the biodistribution of the nanoconstruct at 24 h postinjection, a cohort of the mice were euthanized and representative organs excised for *ex-vivo* fluorescence imaging (Supporting Information, Figure S5B) and analysis (Figure S5C). At this time point, FASOC-UCNPs were mostly distributed in the liver, intestines, lungs and kidneys, with low uptake in the heart and spleen. To assess the tumor selective targeting of the nanoconstruct, mice bearing Bel-7402 tumors (FR-positive) were administrated with FASOC-UCNP-ICG (Figure 6A) or SOC-UCNP-ICG (Figure 6B) and imaged at different time points. Significant tumor uptake was clearly visible in mice treated with FASOC-UCNP-ICG at 4 h postinjection. By 24 postinjection, the maximal tumor fluorescence was attained and the exceptionally high tumor to muscle contrast persisted for more than 96 h postinjection (Figure 6A). Active tumor-targeting of FASOC-UCNP-ICG was also demonstrated in Kunming mice bearing FR-positive S180 tumors (Supporting Information, Figure S5D), indicating the versatility of the nanoconstruct. In contrast, tumor uptake in mice treated with SOC-UCNP-ICG became visible only after 12 h postinjection, which represents the contribution of enhanced permeation and retention in the tumor accumulation of the nanoconstruct. A maximum tumor to skin NIR fluorescence ratio of 11 was attained at 24 h postinjection of FASOC-UCNP-ICG compared with fluorescence ratio of 5.5 for SOC-UCNP-ICG treated mice (Figure 6C). *Ex vivo* fluorescence images of isolated organs/tissues (Figure 6D) confirmed the higher FR-positive tumor targeting ability of FASOC-UCNP than SOC-UCNP. Semiquantitative fluorescence intensity of the isolated tumors from FASOC-UCNP-ICG treated mice is distinctly higher than that of SOC-UCNP-ICG injected mice (Figure 6E), which further supports the FR-mediated high tumor selectivity of FASOC-UCNPs FR-positive tumors. To demonstrate that the detected *in vivo*

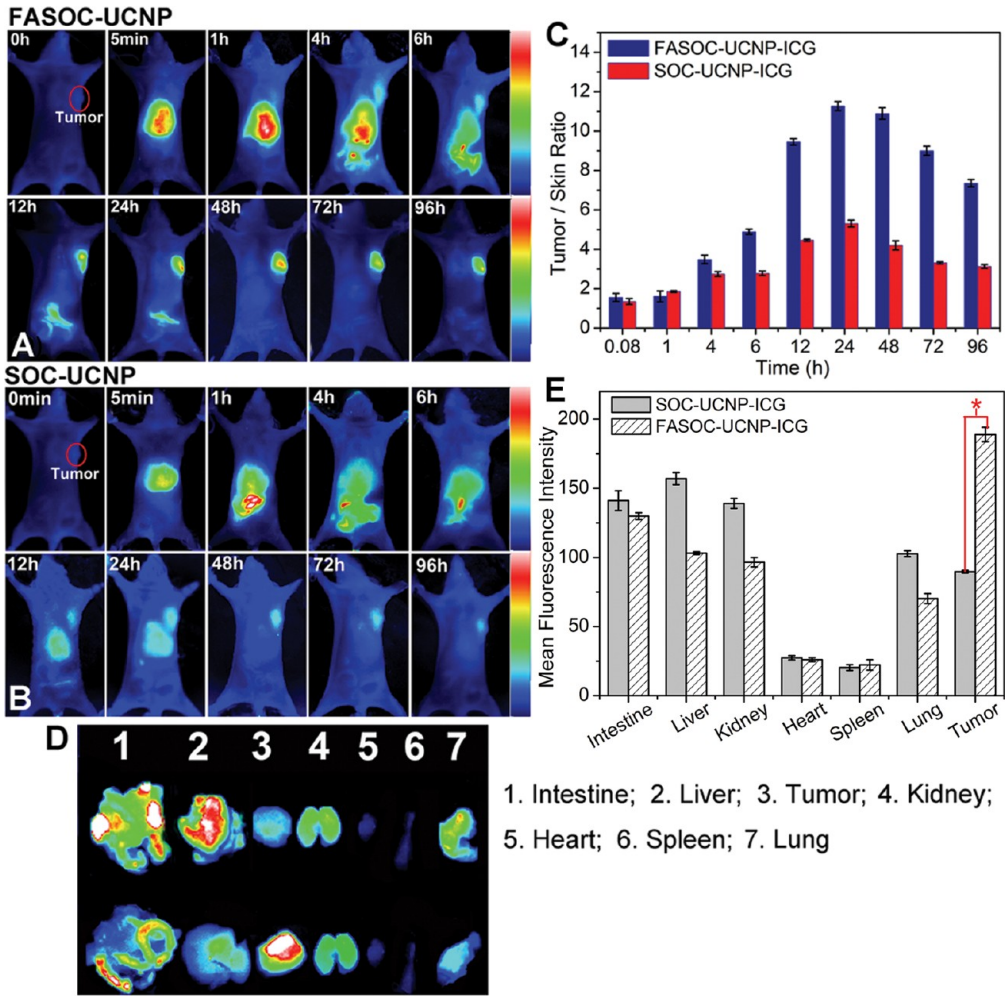

Figure 6. *In vivo* **tumor-targeting of the nanoconstructs. Fluorescence images of nude mice bearing Bel-7402 tumors with intravenously injection of (A) FASOC-UCNP-ICG and (B) SOC-UCNP-ICG; (C) tumor/skin ratio of tumor-bearing mice injected with different nanoconstructs; (D) fluorescence images of isolated organs separated from Bel-7402 tumor-bearing mice in different groups at 24 h postinjection; (E) semiquantification of FASOC-UCNP-ICG and SOC-UCNP-ICG in the isolated organs of mice with different injection.**

fluorescence was associated with the nanoparticles, we investigated the biodistribution of free ICG at the same concentration as the ICG-loaded nanoconstructs in the Bel-7402 tumor-bearing mice (Supporting Information, Figure S5E). The results indicated that the tumor uptake of free ICG molecules was low and the non-encapsulated dye rapidly cleared from the body within 24 h postinjection. After loading into FASOC-UCNPs, a higher ration of the injected ICG accumulated in the tumor, with prolonged retention time of up to 96 h. This suggests that the ICG molecules were trapped in the nanoparticles because the nanoconstructs accumulated in tumors through active ligand targeting and EPR effects (Figure 6A and Supporting Information, Figure S5D). Thus, even if few ICG molecules were separated from the nanoconstructs in the blood circulation, most ICG molecules were retained in the nanoconstructs, as evidenced by the biodistribution of FASOC-UCNP nanoconstructs *in vivo*.

With the tumor uptake of the nanoconstruct having been demonstrated, the deep-penetrating PDT treatment by FASOC-UCNP-ZnPc was explored in S180 tumor-bearing mice using either NIR or red light. Tumor volumes and body weights were recorded for each treated group every other day (Figure 7). The mice treated with saline and FASOC-UCNP-ZnPc without light irradiation did not show any therapeutic effect, as expected. For subcutaneous tumor exposed directly to the 980 or 660 nm light, the measured tumor volumes were identical. To simulate tumors located inside the body, a 1-cm pork tissue was placed on the mouse skin over the subcutaneous tumors during PDT treatment. The result shows that tumor growth significantly decreased in mice exposed to the 980 nm light triggered PDT than those treated with 660 nm (Figure 7A). The tumors were isolated from the different group of mice and weighed on day 14 post-treatment (Table 1). For the subcutaneous tumor, 660 nm PDT shows higher tumor inhibition ratio (77%) than those of

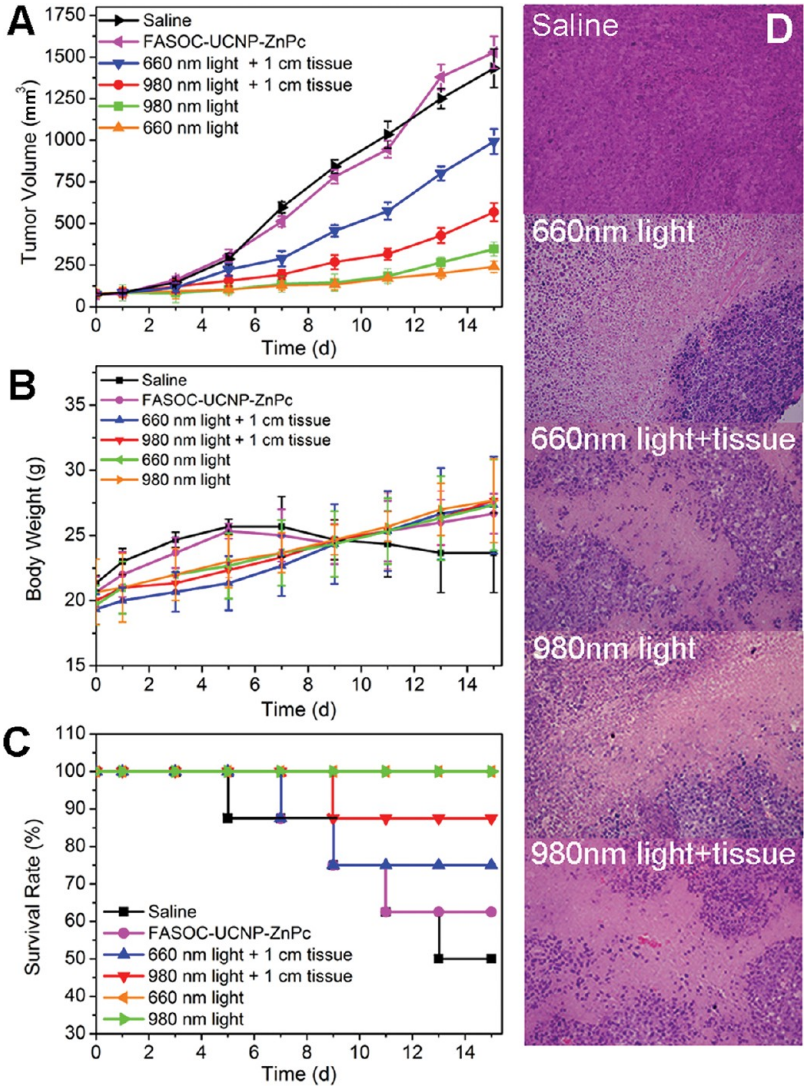

Figure 7. Comparison of the therapeutic efficacy of deep-tissue PDT triggered by 980 and 660 nm light. (A) Tumor growth of mice in different treatment groups within 15 days. (B) Changes of body weight of mice in different groups during PDT. (C) Survival rates of mice in different treatment groups within 15 days. (D) H&E stained tumor tissues harvested from the mice with different treatments.

980 nm triggered PDT treatment (66%). In contrast, the tumor inhibition ratio in the 980 nm PDT group reaches to 50% for the deep tumor model covered with 1-cm tissue, which is obviously higher than that of 660 nm induced treatment (18%). These results demonstrate the advantage of 980 nm triggered PDT for deep-seated tumor treatment.

Body weight and survive rate usually reflect the health condition of the treated mice. As shown in Figure 7B, the body weight of mice in the control group began to decrease from day 9 postinjection, which indicates the living quality of the mice was compromised by the tumor burden. For the PDT treated group, their body weight gradually increased during 15 days, implying that systemic toxicity was minimal in these mice. Survival rates of mice in control and nanoconstruct-treated groups without light irradiation reduce to 50% and 63% at day 15, respectively (Figure 7C).

TABLE 1. Final Tumor Weight and Tumor Inhibition Ratio of Mice in Different Treatment Groups

group	tumor weight (g)	inhibition ratio (%)
control	3.50 ± 0.36	
660 nm light irradiation	0.81 ± 0.31	77
660 nm light +1 cm tissue	2.87 ± 0.26	18
980 nm light irradiation	1.18 ± 0.21	66
980 nm light +1 cm tissue	1.75 ± 0.49	50

None of the mice died in either 660 or 980 nm directly treated group. Survival rates of mice in the deep-penetrating PDT group induced by 660 or 980 nm light irradiation reach to 75% and 88%. These results demonstrate that PDT treatment based on FASOC-UCNP-ZnPc can effectively improve the survival quality of mice and prolong their lifetime. Histological analysis of tumor tissue in different treatment groups at day 7 post-treatment

(Figure 7D) reveals that no damage was found in tumors of control mice. However, markedly increased apoptotic and necrotic tumor cells were observed in all PDT treatment groups, including 660 and 980 nm light-triggered PDT for superficial tumors and deep-seated tumors.

DISCUSSION

This study aims to treat deep-seated tumors by using tumor-targeted UCNP-based PDT nanoconstruct. A high loading of PS to UCNP-based nanoconstructs is typically a prerequisite for efficient *in vivo* PDT treatment through FRET. In this study, we constructed FASOC-coated UCNPs as ZnPc carriers with high drug loading capacity (~10%) through hydrophobic interaction. The previously reported silica-coated UCNPs used as ZnPc carriers suffer from low drug loading capacity (<0.6 wt %) and poor stability of the attached PSs.[16,26] Covalent conjugation of PSs with UCNPs can incorporate over 1000 PS molecules per particle.[18,19] By using a physical encapsulation method, the loading capacity of PEGylated-UCNPs as carriers for Chlorin e6 (Ce6) or meso-tetraphenylporphine (TPP) can reach 8–10 wt %.[15,17] Compared with the reported UCNP-based PDT system, FASOC-UCNP nanoconstructs possess an improved loading capacity for hydrophobic ZnPc molecules. However, the higher loading capacity of ZnPc does not guarantee a better PDT efficiency because there is an optimal loading concentration for ZnPc. Excess ZnPc (250 μg/mL) in the nanoconstructs could not be entirely photoactivated during PDT, and the large number of ZnPc may form aggregates in the FASOC-UCNPs in aqueous media. These conditions would decrease ROS production by increasing the likelihood of deleterious processes such as triplet–triplet annihilation and self-quenching (Supporting Information, Figure S3A).[27] Thus, the optimal loading of ZnPc (150 μg/mL) in the FASOC-UCNP was utilized in the subsequent *in vivo* experiments. A similar result of PS-dependent singlet oxygen production from UCNP-PS complexes has been reported by other researchers.[19] To maximize ROS production from FASOC-UCNP-ZnPc, ZnPc loading should be controlled to avoid aggregation. In future studies, ROS production can be improved by increasing the FRET effect between UCNPs and ZnPc. This can be accomplished by enhancing the upconversion luminescence of UCNPs by silica or $NaYF_4$ coating. In addition, owing to the hydrophobic property and planar structure of ZnPc, it can be efficiently encapsulated in the nanoconstruct with minimal leakage (<20%) even after 50 h incubation at various pH values (5.7, 6.5 and 7.4), which maximized FRET efficiency from UCNP to ZnPc. The good stability of FASOC-UCNP-ZnPc nanoconstruct makes it an excellent UCNP-based PDT system for nonsuperficial tumors.

Safety issues surrounding the use of nanoparticles *in vivo* have become a major obstacle in nanomedicine. To address this problem, the nontoxic and biocompatible SOC was used to coat the UCNP nanoparticle core for this study. In addition to the high stability of the nanoconstruct, our preliminary acute toxicity and biochemistry study of PDT nanoconstruct demonstrates that FASOC-UCNPs display relatively low toxicity and less side effects on the mice, including those injected with high doses of the nanoconstructs (<150 mg/kg, containing 77.5 mg/kg UCNPs). Although the long-term toxicity of UCNPs has been evaluated without any appreciable side effects in the mice injected with low doses of UCNPs (<20 mg/kg).[28] UCNP-based PDT agents for *in vivo* use are best administered under a safe dose (LD50).

Biomolecular recognition moieties such as cyclic arginine–glycine–aspartic acid (RGD) peptide[29] and folic acid[19] are usually conjugated to UCNPs for the targeted PDT of cancer cells. Tumor-targeted UCNP-based PDT agents can effectively increase the accumulation of the nanoparticles and improve PDT efficiency in deep-seated tumors. Very recently, Idris *et al*. first reported the use of targeted upconversion nanoparticles for PDT of subcutaneous tumors, but their treatment programs need long time exposure (2 h) to laser light due to the limited PS loading of silica-coated UCNPs (<0.6 wt %), which might induce photodamage to the tissues.[26] In this study, the well-defined tumor specific ligand FA was covalently conjugated to the surface of UCNPs through the SOC coating. The targeting ability of the FASOC-UCNP-ZnPc nanoconstruct was demonstrated *in vitro* and *in vivo*. The enhanced intracellular uptakes of FASOC-UCNP-ZnPc by FR-positive tumor cells (Bel-7402 and MDA-MB-231) were significantly higher than that in FR-negative A549 tumor cells. This increased uptake is attributed to FR-mediated endocytosis (Figure 4), which is evidenced by FR-blocking experiment in FR-positive cancer cells. In our experiment, a high concentration of free folic acid (1 mM) can effectively inhibit the uptake of folate-modified complexes in FR-positive cells. Similar findings have been reported for FR-mediated tumor targeting of different drugs or nanomaterials in cancer cells and *in vivo* using FR blocking experiments.[30–33] The *in vivo* biodistribution of the UCNP-based nanoconstruct with or without FA modification (Figure 6A, 6B, and Supporting Information, Figure S5D) further confirmed the high tumor targeting ability of FASOC-UCNP in tumor bearing mice. This result suggests that conjugating FA ligands with SOC coating significantly improved the active tumor-targeting of FASOC-UCNP to FR-overexpressed tumors (Bel-7402 and S180).

In general, the main mechanism associated with the killing of cancer cells by PDT is the activation of PSs by light irradiation, which generates cytotoxic ROS that directly destroy the tumor cells.[9] It has been

demonstrated that PDT has two ways to kill cells, defined as Type I and Type II mechanisms.[34] The Type I mechanism involves hydrogen-atom abstraction or electron-transfer reactions between the PS and a substrate to yield free radicals and radical ions, which can interact with molecular oxygen to either generate ROS (such as superoxide anions and hydroxyl radicals) or can cause irreparable biological damage. The Type II mechanism results from an energy transfer between the PS and the molecular oxygen to produce singlet oxygen. DCFH-DA and DPBF probes can detect lethal cytotoxic ROS (not only singlet oxygen) production inside cells and in solution, allowing its use to report the potential PDT efficacy of the nanoconstructs. Unlike visible light, PDT triggered by NIR light enables the feasibility of deep-tissue PDT treatment.[17,18,35,36] Significant light attenuation of 72% and 95% was observed through 1-cm adipose tissue using the same power density (0.2 W/cm^2) at 980 and 660 nm excitation, respectively. Our *in vitro* results (Figure 5) suggest that UCNP-based PDT induced by deep-penetrating 980 nm light produces more ROS than 660 nm light in the cancer cells covered by a 1-cm pork tissue. Although *in vivo* results in Figure 7 indicate 660 nm light-induced PDT possesses better therapeutic efficacy for subcutaneous tumors, NIR-induced PDT using FASOC-UCNP-ZnPc demonstrates superior treatment of simulated 1-cm deep tumors.

CONCLUSION

In this study, we have successfully developed tumor-targeted FASOC-UCNP-ZnPc nanoconstructs with high ZnPc loading capacity for deep-penetrating PDT *in vivo*. Tumor-targeting ability of the nanoconstructs is dramatically enhanced in FR-overexpressed tumors by FR-mediated active targeting. The low toxicity and less side effects of FASOC-UCNP at high dose (<150 mg/kg) are demonstrated in the mice verified by histological and biochemical analysis. Measurement of ROS production under deep tissue both in the solution and in cancer cells reveals that NIR light-triggered PDT by using the nanoconstructs generates more ROS in contrast to direct irradiation of ZnPc upon 660 nm light. In comparison with conventional PDT depending on red light irradiation, the NIR-induced PDT based on the nanoconstructs possesses higher tumor inhibition ratio for the treatment of simulated deep-seated tumors. Together, our results demonstrate the considerable advantages of tumor-selective UCNP-based PDT induced by NIR light over traditional PDT for internal tumors and prompt further explorations of these nanoconstructs for targeted drug delivery and deep-tissue PDT of other related diseases.

MATERIALS AND METHODS

Materials. RE_2O_3 (RE = Y, Yb, and Er) were purchased from Aladdin Reagent Company and Sinopharm Chemical Reagent Co. Ltd. $RECl_3$ were prepared by dissolving the corresponding RE_2O_3 in hydrochloric acid solution. The products were evaporated and redissolved in distilled water. Zinc(II) phthalocyanine (ZnPc, 95%, Alfa Aesar), 1,3-diphenylisobenzofuran (DPBF, 97%, Sigma-Aldrich), Annexin V-FITC Apoptosis Detection Kit (Sigma-Aldrich), 2′,7′-dichlorfluorescein-diacetate (DCFH-DA) reactive oxygen species assay kit (Beyotime), oleic acid (OA, 90%, Aladdin), 1-octadecen (ODE, 90%, Aladdin), folic acid (Sinopharm Chemical Reagent Co. Ltd.), Hoechst 33342 (Beyotime) and 3-(4,5-dimethylthiazol-2-yl)-2,5-diphenyltetrazolium bromide (MTT, 98%, Aladdin) were used as received without further purification.

Preparation of FASOC-UCNP-ZnPc. $NaYF_4$ (Y:Yb:Er = 0.78:0.2:0.02) nanoparticles and *N*-succinyl-*N*′-octyl chitosan (SOC, 5 KDa) were synthesized as reported previously.[20,22,30] FASOC was prepared by covalently conjugating folic acid to the amino groups of SOC. Briefly, folic acid (0.22 g) was activated with *N*-hydroxysuccimide (NHS) and dicyclohexylcarbodiimide (DCC) at 50 °C for 6 h (FA/NHS/DCC molar ratio = 1:1:1.5). The precipitate was removed by filtration (0.22 μm) and the NHS-FA was precipitated by acetone and diethyl ether (V/V = 3:7). The activated FA (30 mg) was reacted with aqueous solution of SOC (4 mg/mL, 5 mL) at room temperature for 24 h. The mixture was dialyzed (MWCO 8000−14000) against phosphate buffer solution (PBS) and was centrifuged (8000 rpm, 10 min) to remove excess NHS-FA. The structure of the FASOC conjugate has determined by ^{1}H NMR in our previous report.[30] The prepared UCNPs (0.5 mg) were redispersed in FASOC aqueous solution (2 mg/mL) by sonication (*P* = 100 W). The obtained colloid solution was filtered through 0.22 μm filter to remove large aggregates. Thereafter, different amounts of ZnPc in DMSO solution (50−500 μM) were added into 2 mL of FASOC-UCNPs aqueous solution and stirred overnight. Free ZnPc was removed by centrifugation at 14000 rpm for 20 min. The obtained precipitate (FASOC-UCNP-ZnPc) was washed with distilled water (3×) and resuspended in distilled water by sonication to form a homogeneous colloidal solution.

Drug Loading and Encapsulation Efficiency. ZnPc drug loading capacity and encapsulation efficiency in the FASOC-UCNPs were determined by fluorospectrophotometry, setting the excitation wavelength at 610 nm and monitoring the fluorescence emission in the range of 650−750 nm.[20,24] The concentration of ZnPc was calculated by means of a calibration curve, which was performed in triplicate (*n* = 3) covering the range of 0.02−0.80 μM ZnPc in ethanol. A certain amount of FASOC-UCNP-ZnPc was diluted by ethanol to the range covered within standard curve. The ZnPc was extracted from the FASOC-UCNPs by ethanol by centrifugation at 12000 rpm for 15 min to remove the chitosan and UCNP precipitates and the ZnPc content in the supernatant was measured by spectrofluorimetry. The extraction efficiency was about 97%, which is defined as the ratio of fluorescence intensity of ZnPc extracted from the nanoconstructs to the fluorescence intensity of total ZnPc in the nanoconstructs. The measurement was carried out in triplicate for each formulation (*n* = 3). Drug loading capacity of ZnPc (%) was calculated as follows: loading capacity = [amount of ZnPc in the FASOC-UCNPs (g)]/[amount of FASOC-UCNP-ZnPc (g)] × 100. Encapsulation efficiency (%) was calculated as follows: encapsulation efficiency = [amount of ZnPc in the FASOC-UCNPs (g)]/[total amount of ZnPc (g)] × 100.

***In Vitro* Drug Release.** ZnPc release kinetic analysis was performed following a modified method in ref 24. In brief, 1 mL of FASOC-UCNP-ZnPc (2 mg/mL) was dispersed in 50 mL of PBS containing 2% SDS at 37 °C with continuous stirring. A 3 mL amount of solution was withdrawn and centrifuged at 12000 rpm for 10 min at different time points. ZnPc in the supernatant was measured by spectrofluorimetry which is similar to the condition described above; however, the standard

curve of ZnPc in the range of 0.02−0.40 μM was calibrated in phosphate buffer at various pH values (5.7, 6.5, and 7.4) containing 2% SDS. The precipitates were resuspended in 3 mL of fresh medium and placed in the releasing sample again. The concentration of ZnPc released from the FASOC-UCNPs was calculated by using the peak area of ZnPc emission (650−750 nm) in PBS.

Characterization. Morphology and size of the prepared nanoparticles were characterized by using a JEOL JEM-2100 high-resolution transmission electron microscope (HR-TEM). Dynamic light scattering (DLS) was performed by a Brookhaven Nanoparticle Size Analyzer to measure the hydrodynamic diameter. Fourier transform infrared spectra were determined by a BRUKER-MPA spectrophotometer. The PL spectra were measured by a F96 fluorescence spectrophotometer (Lengguang Technology Co. LTD, China) with a xenon lamp and an external 980 nm laser (Scitower Photoelectricity Equipment Co. LTD, China). The UV−vis absorption spectra were acquired by a 754-PC UV−vis spectrophotometer (JingHua technological instrument corporation, China). All optical measurements were performed at room temperature.

Cellular Uptake and FR Blocking Experiments. Human hepatocellular carcinoma Bel-7402 cells (folate receptor (FR)-positive), human breast carcinoma MDA-MB-231 cells (FR-positive), human lung adenocarcinoma A549 cells (FR-negative), and human embryo lung cells (HELF) were purchased from American Type Culture Collection (ATCC, USA). The cells were originally cultured in RPMI-1640 medium supplemented with 10% (v/v) calf serum, penicillin (100 U/mL), and (100 μg/mL) streptomycin. Cells were maintained at 37 °C in a humidified atmosphere containing 5% CO_2.

To investigate the targeted drug delivery of ZnPc by FASOC-UCNPs in the cells, intracellular uptake of FASOC-UCNP-ZnPc and the receptor blocking experiment were performed with the FR-positive Bel-7402 and MDA-MB-231 cells and FR-negative A549 cells. Three cell lines were in the confocal dishes at a density of 3×10^5 cells/dish. After 24 h of cell attachment, 200 μL of FASOC-UCNP-ZnPc (containing 100 μM ZnPc) was added in the culture medium and incubated for different times (1, 3, 7, and 10 h). Cell nuclei were stained with Hoechst 33342 (μg/mL) for 30 min. After washing three times with PBS, the cells were imaged by a laser confocal microscope (Olympus FV1100, Japan). UCL imaging of FASOC-UCNP-ZnPc was performed by using confocal microscope equipped with an external 980 nm laser. In the FR receptor blocking experiment, Bel-7402 and MDA-MB-231 cancer cells (3×10^5 cells/dish) were first incubated with free FA (1 mM) for 30 min and then 200 μL of FASOC-UCNP-ZnPc (containing 57 μg/mL ZnPc) was added in the medium. As a control, the cells were directly incubated with the nanoconstructs without blocking the FR. After 2 h incubation, cell nuclei were stained with Hoechst 33342 for 30 min and then the cells were washed three times with PBS for fluorescence confocal imaging.

Intracellular ROS Detection. ROS generation inside cells was detected using DCFH-DA Reactive Oxygen Species Assay Kit. Bel-7402 cells were seeded in confocal dishes at a density of 3×10^5 cells/dish. Following incubation with FASOC-UCNP-ZnPc for 24 h, DCFH-DA was loaded into the cells. After 30 min incubation, cells were washed twice with PBS and then exposed to 980 or 660 nm irradiation for 10 min at the power density of 0.2 W/cm^2. To compare ROS production of 980 and 660 nm light in deep tissue, cell dishes were covered with 1-cm adipose tissues and then irradiated with the two lights under the same condition as above. After irradiation, fluorescence images of treated cells were acquired using a laser confocal microscope.

Acute Toxicity Experiment. To evaluate acute toxicity of the prepared nanoconstructs in mice, a total of 35 healthy Kunming mice (male and female, half and half) were randomly assigned in five groups and intravenously injected with 300 μL of FASOC-UCNP-ZnPc (0, 36, 51.45, 73.5, 105, 150, 220 mg/kg, containing 0, 18.7, 26.7, 38.2, 54.5, 78, 115 mg/kg of comparable $NaYF_4$:Yb, Er UCNPs), respectively. The mice were weighed every day to note any weight variation and survival rates were recorded for 7 days. Blood samples were collected from the orbital sinus by quickly removing the eyeball from the mice at the 7th day after injection.

***In Vivo* Dynamic Distribution and Tumor-Targeting of the Nanoconstruct.** Female athymic nude mice and normal (Kunming) mice were purchased from Charles River Laboratories (Shanghai, China). All animal experiments were carried out in compliance with the Animal Management Rules of the Ministry of Health of the People's Republic of China and the guidelines for the Care and Use of Laboratory Animals of China Pharmaceutical University. Bel-7402 and S180 cells (5×10^6) were subcutaneously injected into the upper left axillary fossa in the nude mice or Kunming mice ($n = 8$). As the tumors grew up to a diameter of 0.4−0.5 cm, the mice were used for NIR imaging and PDT treatment.

NIR dye ICG-Der-01 was encapsulated in the nanoconstructs (FASOC-UCNP-ICG). FASOC-UCNP-ICG (20 mg/kg; 0.2 mL) was injected through the tail vein into Bel-7402 tumor-bearing nude mice and Kunming mice bearing S180 tumors. Fluorescence images of the mice were acquired by the NIR imaging system at different time points postinjection. Background images were taken for each mouse prior to injection.

***In Vivo* PDT Treatment.** Mice bearing S180 tumors were randomly assigned into three groups ($n = 8$), when the tumor grew up to a diameter of 0.5 cm. The mice in each group were treated with saline or FASOC-UCNP-ZnPc (50 mg/kg, containing 2.88 mg/kg ZnPc) *via* intravenous injection. After 24 h post-injection, the mice in the experimental groups were treated with different therapeutic schedules: (1) PDT triggered by 980 nm light (0.2 W/cm^2, 30 min); (2) PDT induced 660 nm light (0.2 W/cm^2, 30 min); (3) 980 nm light triggered PDT for tumors in deep tissue (0.2 W/cm^2, 30 min); (4) 660 nm light induced PDT for tumors in deep tissue (0.2 W/cm^2, 30 min). Saline-treated mice without light irradiation were studied as control. The therapeutic efficacy of FASOC-UCNP-ZnPc on mice bearing a S180 tumor was assessed by measuring tumor volume, body weight, and survival rate of mice in each group every other day. Tumor volume was calculated as length $\times$ (width)$^2 \times {}^1/_2$. All mice were killed and the tumors were collected 14 days after treatment. Tumor inhibition ratio (%) = $((W_c - W_t)/W_c) \times 100$, where W_c and W_t are the average tumor weight of control group and treatment group, respectively.

Histology Examination. To confirm the PDT efficacy of FASOC-UCNP-ZnPc for tumor therapy, histology analysis of tumor tissues was performed after treatment. Tumor tissues in the control group and PDT treatment groups were separated and fixed with 10% neutral buffered formalin and embedded in paraffin ($n = 5$). The sliced organs were stained with H&E and examined under a microscope.

Statistical Analysis. Significant differences were determined using the Student's t test where differences were considered significant ($p < 0.05$). All data are expressed as mean ± standard error of the mean.

Conflict of Interest: The authors declare no competing financial interest.

Acknowledgment. This research was supported by the Natural Science Foundation Committee of China (NSFC 30970776, 81000666, 81071194, 81171395, and 81220108012), the major project from the Ministry of Science and Technology for new drug development (2009ZX09310-004).

Supporting Information Available: Methods of MTT assays for cytotoxicity and determination of ROS in the solution). Cytotoxic study of the nanoconstructs in cancer cells. Folate receptor expression in different cancer cells determined by RT-PCR. ROS production of FASOC-UCNP-ZnPc in solution detected by DPBF. Acute toxicity study in the mice. *In vivo* dynamic distribution, tumor-targeting of the nanoconstructs in S180 tumor-bearing mice and tumor-targeting of free ICG-Der-01 in Bel-7402 tumor-bearing mice. This material is available free of charge *via* the Internet at http://pubs.acs.org.

REFERENCES AND NOTES

1. Juarranz, A.; Jaen, P.; Sanz-Rodriguez, F.; Cuevas, J.; Gonzlez, S. Photodynamic Therapy of Cancer. Basic Principles and Applications. *Clin. Transl. Oncol.* **2008**, *10*, 148–154.
2. Celli, J. P.; Spring, B. Q.; Rizvi, I.; Evans, C. L.; Samkoe, K. S.; Verma, S.; Pogue, B. W.; Hasan., T. Imaging and Photodynamic

Therapy: Mechanisms, Monitoring, and Optimization. *Chem. Rev.* **2010**, *110*, 2795–2838.
3. Konan, Y. N.; Gurny, R.; Allemann, E. State of the Art in the Delivery of Photosensitizers for Photodynamic Therapy. *J. Photochem. Photobiol. B* **2002**, *66*, 89–106.
4. Detty, M. R.; Gibson, S. L.; Wagner, S. J. Current Clinical and Preclinical Photosensitizers for Use in Photodynamic Therapy. *J. Med. Chem.* **2004**, *47*, 3897–3915.
5. Zhang, P.; Steelant, W.; Kumar, M.; Scholfield, M. Versatile Photosensitizers for Photodynamic Therapy at Infrared Excitation. *J. Am. Chem. Soc.* **2007**, *129*, 4526–4527.
6. Chatterjee, D. K.; Zhang, Y. Upconverting Nanoparticles as Nanotransducers for Photodynamic Therapy in Cancer Cells. *Nanomedicine (London)* **2008**, *3*, 73–82.
7. Wang, F.; Banerjee, D.; Liu, Y. S.; Chen, X. Y.; Liu, X. G. Upconversion Nanoparticles in Biological Labeling, Imaging, and Therapy. *Analyst* **2010**, *135*, 1839–1854.
8. Guo, H.; Qian, H.; Idris, N. M.; Zhang, Y. Singlet Oxygen-Induced Apoptosis of Cancer Cells Using Upconversion Fluorescent Nanoparticles as a Carrier of Photosensitizer. *Nanomedicine* **2009**, *6*, 486–495.
9. Hackbarth, S.; Schlothauer, J.; Preuss, A.; Roder, B. New Insights to Primary Photodynamic Effects—Singlet Oxygen Kinetics in Living Cells. *J. Photochem. Photobiol. B* **2010**, *98*, 173–179.
10. Chatterjee, D. K.; Fong, L. S.; Zhang, Y. Nanoparticles in Photodynamic Therapy: An Emerging Paradigm. *Adv. Drug Delivery Rev.* **2008**, *60*, 1627–1637.
11. Paszko, E.; Ehrhardt, C.; Senge, M. O.; Kelleher, D. P.; Reynolds, J. V. Nanodrug Applications in Photodynamic Therapy. *Photodiagn. Photodyn. Ther.* **2011**, *8*, 14–29.
12. Chen, B.; Pogue, B. W.; Hasan, T. Liposomal Delivery of Photosensitizing Agents. *Expert Opin. Drug Delivery* **2005**, *2*, 477–487.
13. Rossi, L. M.; Silva, P. R.; Vono, L. L.; Fernandes, A. U.; Tada, D. B.; Baptista, M. S. Protoporphyrin IX Nanoparticle Carrier: Preparation, Optical Properties, and Singlet Oxygen Generation. *Langmuir* **2008**, *24*, 12534–12538.
14. Lee, S. J.; Koo, H.; Jeong, H.; Huh, M. S.; Choi, Y.; Jeong, S. Y.; Byun, Y.; Choi, K.; Kim, K.; Kwon, I. C. Comparative Study of Photosensitizer Loaded and Conjugated Glycol Chitosan Nanoparticles for Cancer Therapy. *J. Controlled Release* **2011**, *152*, 21–29.
15. Shan, J. N.; Budijono, S. J.; Hu, G.; Yao, N.; Kang, Y.; Ju, Y.; Prud'homme, R. K. Pegylated Composite Nanoparticles Containing Upconverting Phosphors and Meso-Tetraphenyl Porphine (TPP) for Photodynamic Therapy. *Adv. Funct. Mater.* **2011**, *21*, 2488–2495.
16. Qian, H.; Guo, H.; Ho, P.; Mahendran, R.; Zhang, Y. Mesoporous-Silica-Coated Upconversion Fluorescent Nanoparticles for Photodynamic Therapy. *Small* **2009**, *5*, 2285–2290.
17. Wang, C.; Tao, H.; Cheng, L.; Liu, Z. Near-Infrared Light Induced *in Vivo* Photodynamic Therapy of Cancer Based on Upconversion Nanoparticles. *Biomaterials* **2011**, *32*, 6145–6154.
18. Park, Y. I.; Kim, H. M.; Kim, J. H.; Moon, K. C.; Yoo, B.; Lee, K. T.; Lee, N.; Choi, Y.; Park, W.; Ling, D.; *et al*. Theranostic Probe Based on Lanthanide-Doped Nanoparticles for Simultaneous *in Vivo* Dual-Modal Imaging and Photodynamic Therapy. *Adv. Mater.* **2012**, *24*, 5755–5761.
19. Liu, K.; Liu, X.; Zeng, Q.; Zhang, Y.; Tu, L.; Liu, T.; Kong, X.; Wang, Y.; Cao, F.; Lambrechts, S. A.; *et al*. Covalently Assembled NIR Nanoconstruct for Simultaneous Fluorescence Imaging and Photodynamic Therapy of Cancer Cells. *ACS Nano* **2012**, *6*, 4054–4062.
20. Cui, S.; Chen, H.; Zhu, H.; Tian, J.; Qian, Z.; Achilefu, S.; Gu, Y. Amphiphilic Chitosan Modified Upconversion Nanoparticles for *in Vivo* Photodynamic Therapy Induced by Near-Infrared Light. *J. Mater. Chem.* **2012**, *22*, 4861–4873.
21. Cho, K.; Wang, X.; Nie, S.; Chen, Z.; Shin, D. M. Therapeutic Nanoparticles for Drug Delivery in Cancer. *Clin. Cancer Res.* **2008**, *14*, 1310–1316.
22. Li, Z.; Zhang, Y. An Efficient and User-Friendly Method for the Synthesis of Hexagonal-Phase $NaYF_4$:Yb, Er/Tm Nanocrystals with Controllable Shape and Upconversion Fluorescence. *Nanotechnology* **2008**, *19*, 345606.
23. Guo, J.; Du, C.; Shan, L.; Zhu, H.; Xue, B.; Qian, Z.; Achilefu, S.; Gu, Y. Comparison of Near-Infrared Fluorescent Deoxyglucose Probes with Different Dyes for Tumor Diagnosis *in Vivo*. *Contrast Media Mol. Imaging* **2012**, *7*, 289–301.
24. Ricci-Junior, E.; Marchetti, J. M. Zinc(II) Phthalocyanine Loaded PLGA Nanoparticles for Photodynamic Therapy Use. *Int. J. Pharm.* **2006**, *310*, 187–195.
25. Zeng, H.; Korbelik, M.; McLean, D. I; MacAulay, C.; Harvey, H. Monitoring Photoproduct Formation and Photobleaching by Fluorescence Spectroscopy Has the Potential to Improve PDT Dosimetry with a Verteporfin-like Photosensitizer. *Photochem. Photobiol.* **2002**, *75*, 398–405.
26. Idris, N. M.; Gnanasammandhan, M. Kumara.; Zhang, J.; Ho, P. C.; Mahendran, R.; Zhang, Y. *In Vivo* Photodynamic Therapy Using Upconversion Nanoparticles as Remote-Controlled Nanotransducers. *Nat. Med.* **2012**, *18*, 1580–1585.
27. Hotze, E. M.; Labille, J.; Alvarez, P.; Wiesner, M. R. Mechanisms of Photochemistry and Reactive Oxygen Production by Fullerene Suspensions in Water. *Environ. Sci. Technol.* **2008**, *42*, 4175–4180.
28. Cheng, L.; Yang, K.; Shan, M.; Lu, X.; Liu, Z. *In Vivo* Pharmacokeinetics, Long-Term Biodistribution and Toxicology Study of Functional Upconversion Nanoparticles in Mice. *Nanomedicine (Lond)* **2011**, *6*, 1327–1340.
29. Zhou, A.; Wei, Y.; Wu, B.; Chen, Q.; Xing, D.; Pyropheophorbide, A. and c(RGDyK) Comodified Chitosan-Wrapped Upconversion Nanoparticle for Targeted Near-Infrared Photodynamic Therapy. *Mol. Pharm.* **2012**, *9*, 1580–1589.
30. Zhu, H. Y.; Liu, F.; Guo, J.; Xue, J.; Qian, Z.; Gu, Y. Folate-Modified Chitosan Micelles with Enhanced Tumor Targeting Evaluated by Near Infrared Imaging System. *Carbohydr. Polym.* **2011**, *86*, 1118–1129.
31. Sudimack, J.; Lee, R. J. Targeted Drug Delivery *via* the Folate Receptor. *Adv. Drug Delivery Rev.* **2000**, *41*, 147–162.
32. Song, E. Q.; Zhang, Z. L.; Luo, Q. Y.; Lu, W.; Shi, Y. B.; Pang, D. W. Tumor Cell Targeting Using Folate-Conjugated Fluorescent Quantum Dots and Receptor-Mediated Endocytosis. *Clin Chem.* **2009**, *55*, 955–63.
33. Manasi, D.; Sanjeeb, K. S. Folate Decorated Dual Drug Loaded Nanoparticle: Role of Curcumin in Enhancing Therapeutic Potential of Nutlin-3a by Reversing Multidrug Resistance. *PLoS One* **2012**, *7*, e32920.
34. Sharman, W. M.; Allen, C. M.; van Lier, J. E. Photodynamic Therapeuties: Basic Principles and Clinical Applications. *Drug Discovery Today* **1999**, *4*, 507–517.
35. Jayakumar, M. K.; Idris, N. M.; Zhang, Y. Remote Activation of Biomolecules in Deep Tissues Using Near-Infrared-to-UV Upconversion Nanotransducers. *Proc. Natl. Acad. Sci. U.S.A.* **2012**, *109*, 8483–8488.
36. Chatterjee, D. K.; Gnanasammandhan, M. K.; Zhang, Y. Small Upconverting Fluorescent Nanoparticles for Biomedical Applications. *Small* **2010**, *6*, 2781–2795.